

1                   **Estimating radiative forcing with a nonconstant**  
2                   **feedback parameter and linear response**

3                   **Hege-Beate Fredriksen<sup>1</sup>, Maria Rugenstein<sup>2</sup> and Rune Graversen<sup>1,3</sup>**

4                   <sup>1</sup>Department of Physics and Technology, UiT the Arctic University of Norway, Tromsø, Norway

5                   <sup>2</sup>Colorado State University, Fort Collins, USA

6                   <sup>3</sup>The Norwegian Meteorological Institute, Norway

7                   **Key Points:**

- 8                   • We present a new method for estimating effective radiative forcing and apply it  
9                   to abrupt4xCO<sub>2</sub>, historical, and future scenario experiments  
10                  • Including a time-scale dependent feedback parameter results in stronger forcing  
11                  estimates for the 21st century  
12                  • The temperature responses to the new forcing are well described by a linear re-  
13                  sponse

---

Corresponding author: Hege-Beate Fredriksen, [hege-beate.fredriksen@uit.no](mailto:hege-beate.fredriksen@uit.no)

**Abstract**

A new algorithm is proposed for estimating time-evolving global forcing in climate models. The method is a further development of the work of Forster et al. (2013), taking into account the non-constancy of the global feedbacks. We assume the non-constancy of this global feedback can be explained as a time-scale dependence, associated with linear temperature responses to the forcing on different time scales. With this method we obtain stronger forcing estimates than previously assumed for the representative concentration pathway experiments in the Coupled Model Intercomparison Project Phase 5 (CMIP5). The reason for the higher future forcing is that the global feedback parameter is more negative at shorter time scales than at longer time scales, consistent with the equilibrium climate sensitivity increasing with equilibration time. Our definition of forcing provides a clean separation of forcing and response, and we find that linear temperature response functions estimated from experiments with abrupt quadrupling of CO<sub>2</sub> can be used to predict responses also for future scenarios. In particular, we demonstrate that applying this response to our new forcing estimate predicts the modelled response up to year 2100 quite well for most models.

**1 Introduction**

Diagnosing the magnitude of a climate forcing is necessary for determining the climate responses to this forcing. However, defining a clear separation between forcing and response is challenging, and no clear distinction exists (Sherwood et al., 2015). In this paper we attempt to apply a separation within a linear temperature response framework, also incorporating the possibility of globally nonconstant atmospheric feedbacks. We test this method on models participating in the Coupled Model Intercomparison Project Phase 5 (CMIP5).

In the most common forcing-feedback framework, the radiative imbalance at the top of the atmosphere ( $N$ ) is described as

$$N = \lambda T + F \tag{1}$$

where  $T$  is the temperature response,  $\lambda$  is the feedback parameter, and  $F$  is the radiative forcing, all evaluated as the global mean. According to this equation, forcing is the initial radiative imbalance, before the global mean surface temperature starts to respond. However, as discussed by Hansen et al. (2005), there are many ways of defining the forcing, including various fast feedbacks before diagnosing the radiative imbalance. Forcing estimates are therefore method and model dependent. Some studies even consider multi-annual adjustments to the application of the forcing, reaching into the ocean (Williams et al., 2008; Rugenstein, Gregory, et al., 2016; Menzel & Merlis, 2019). A main motivation for this study is therefore to find an estimation method aiming for a clean separation between forcing and response.

The uncertainties associated with forcing estimates are large, not just because of the different fast feedbacks between models, but also largely due to differences in the parameterizations of the radiative transfer (Soden et al., 2018). The instantaneous forcing spread contributes to about half of the total intermodel spread in forcing (Chung & Soden, 2015), and the remaining spread is largely due to fast cloud adjustments (Zelinka et al., 2013). These uncertainties have led to a large effort aiming to better characterize the forcing used for the new CMIP6 model versions (Forster et al., 2016; Pincus et al., 2016).

In experiments with a time-varying forcing, forcing estimates may be even more uncertain than in idealized experiments with constant forcing. Forster et al. (2013), hereafter F13, computes forcing time series  $F(t)$  by rearranging Eq. (1). Their method consists of first determining  $\lambda$  following the regression method of Gregory et al. (2004) using idealized step-forcing simulations, and then using time series of  $N(t)$  and  $T(t)$  from

any experiment to compute what they call adjusted forcing:

$$F(t) = N(t) - \lambda T(t) \quad (2)$$

56 We note that adjusted forcing in F13 does not mean the same as adjusted forcing  
 57 in Hansen et al. (2005), where the latter allows only fast stratospheric adjustments to  
 58 take place before the forcing is estimated from the top of the atmosphere imbalance in  
 59 an idealized step-forcing experiment. Forcing estimates based on regressions in a Gre-  
 60 gory plot, such as in Andrews et al. (2012) and F13 are what Forster et al. (2016) refers  
 61 to as regression-based methods, assuming a constant feedback parameter.

62 But several recent studies have pointed out that  $\lambda$  is not a constant (Armour et  
 63 al., 2013; Geoffroy, Saint-Martin, Bellon, et al., 2013; Andrews et al., 2015; Gregory &  
 64 Andrews, 2016; Proistosescu & Huybers, 2017; Rugenstein et al., 2020). Armour et al.  
 65 (2013) demonstrate that locally constant feedbacks can result in a globally time-dependent  
 66 feedback parameter because the pace of sea surface temperatures (SST) equilibration de-  
 67 pends on the location, weighting the local feedbacks. Other studies demonstrated that  
 68 also locally, feedbacks change their magnitude with equilibration time (e.g. Andrews et  
 69 al., 2015; Andrews & Webb, 2018; Rugenstein, Caldeira, & Knutti, 2016; Proistosescu  
 70 & Huybers, 2017; Rugenstein et al., 2020) and also throughout the historical time pe-  
 71 riod (Paynter & Frölicher, 2015; Gregory & Andrews, 2016; Armour, 2017; Marvel et al.,  
 72 2018; Dessler, 2020). The entire Tropics, the tropical Pacific specifically, the east-west  
 73 gradient in the tropical Pacific, the relative warming of midlatitude or global oceans to  
 74 the West Pacific warm pool, the North Atlantic, and the mid- and high latitudes have  
 75 all been suggested to influence global feedbacks strongly (e.g. Winton et al., 2010; Tross-  
 76 sman et al., 2016; Andrews & Webb, 2018; Dong et al., 2020; Zelinka et al., 2020). The  
 77 mechanism most often invoked is the dependence of lower tropospheric stability on the  
 78 ratio of local and far-field SSTs. Regions warming faster than the West Pacific warm pool  
 79 — which sets the temperature of the free troposphere through deep convective clouds  
 80 — show a reduced lower tropospheric stability, a decrease in low-cloud coverage, and thus,  
 81 a strong cloud and net radiative effect at the top of the atmosphere (e.g. Zhou et al.,  
 82 2016; Ceppi & Gregory, 2017). In the CMIP6 models, the shortwave cloud feedbacks in  
 83 the extratropics appear to be more important for the nonconstancy of  $\lambda$  than clouds in  
 84 the tropics (Zelinka et al., 2020; Bacmeister et al., 2020), but the relatively short record  
 85 of global cloud observations makes it difficult to assess cloud modeling against the ob-  
 86 servations (Loeb et al., 2020). Some studies explain also the changing feedback strength  
 87 as a temperature-dependence (Meraner et al., 2013; Rohrschneider et al., 2019; Bloch-  
 88 Johnson, Rugenstein, Stolpe, et al., 2020).

89 The nonconstancy of  $\lambda$  implies that the forcing definition in Eq. (2) is ambiguous.  
 90 This is particularly apparent for strong temperature responses, when  $\lambda T$  more strongly  
 91 affects the determination of the value of  $F$ . Here the magnitude and time-dependence  
 92 of  $\lambda$  are particularly important. Larson and Portmann (2016) demonstrated for instance  
 93 that  $\lambda$  obtained from regressions in the first 20 yr time period of abrupt4xCO<sub>2</sub> gives higher  
 94 forcing estimates compared to regressions in 150 yr time period. This is one of several  
 95 reasons why Forster et al. (2016) recommends fixed-SST methods instead of regression  
 96 methods to determine the forcing.

97 We explore how an alternative definition of effective forcing with a time-scale de-  
 98 pendent  $\lambda$  differs from estimates by F13. To compute these alternative estimates, we de-  
 99 compose the temperature response assuming it responds linearly to the forcing, and we  
 100 demonstrate that the linear temperature response to the new forcing is close to the mod-  
 101 elled temperature response in future scenarios for most CMIP5 models. By a linear re-  
 102 sponse, we mean the temperature response determined from a linear non-homogeneous  
 103 system of differential equations, whose solution can be expressed as a convolution be-  
 104 tween a Green’s function and the forcing. Our results suggest that this forcing estimate

105 appears more appropriate for estimating temperature responses using linear response mod-  
 106 els.

107 Our method is an iterative routine, starting with the F13 estimate of forcing, then  
 108 computing the linear response to this forcing, which is further used to compute a new  
 109 forcing estimate, etc., until convergence to a final forcing estimate is obtained. Theory  
 110 and methods are described in Section 2, and the results are shown in Section 3. In Sec-  
 111 tion 4, we discuss the assumptions made in our method, and how it compares to other  
 112 forcing estimates, before we conclude in Section 5.

## 113 2 Theory and methods

The time-scale dependence of  $\lambda$  is analysed by making use of the same decompo-  
 sition as in Proistosescu and Huybers (2017), hereafter PH17. While PH17 use the method  
 to better understand estimates of climate sensitivity, we are interested in the intersect  
 of the fit with the vertical axis, the initial radiative imbalance. We also estimate param-  
 eters using a different approach, mainly because our method simplifies the comparison  
 to methods based on single regression estimates in Gregory plots. The equations that  
 will be presented in this section provide interpretations of the different  $\lambda$ 's that may ap-  
 pear in a Gregory plot, as well as interpretations of "forcing estimates" based on regres-  
 sions on the long time scales. The method is based on the assumption that the temper-  
 ature response can be decomposed into a sum of  $K$  components  $T = \sum_{n=1}^K T_n$ , where  
 each component is the exponential temperature response to the forcing on the time scale  
 $\tau_n$ ,

$$T_n(t) = c_n \exp(-t/\tau_n) * F(t). \quad (3)$$

114 The \* denotes a convolution, and the factors  $c_n$  are the amplitudes of the temperature  
 115 responses per unit forcing. As further explained in the next subsection, this tempera-  
 116 ture decomposition can be interpreted as a combination of having different responses in  
 117 different regions, and that regions responds to forcing on different time scales.  $c_n$  there-  
 118 fore depends on both the feedbacks and thermal inertia associated with different regions,  
 119 and the fraction of the global area involved in the response at time scale  $\tau_n$ .

Furthermore, the method assumes that constant feedback parameters  $\lambda_n$  exist, with  
 $n = 1, \dots, K$  associated with each time scale, such that the terms in Eq. (1) can be de-  
 composed into the following sums:

$$N(t) = \sum_{n=1}^K N_n(t) = F(t) + \sum_{n=1}^K \lambda_n T_n(t) = F(t) + \lambda(t)T(t) \quad (4)$$

By rewriting Eq. (4), PH17 noted that the time-variation of  $\lambda(t)$  can be explained  
 as a weighted average of the feedbacks associated with different components  $T_n(t)$  of the  
 global temperature:

$$\lambda(t) = \frac{\sum_{n=1}^K \lambda_n T_n(t)}{\sum_{n=1}^K T_n(t)} \quad (5)$$

120 We note that in a  $4xCO_2$  experiment, we define the forcing to be a constant, and  
 121 the slope  $\lambda(t)$  must be interpreted as the slope of a line drawn between the fixed forc-  
 122 ing  $F$  and a point  $(T(t), N(t))$ . This slope may differ from a linearization around a point  
 123  $(T(t), N(t))$ , e.g. slopes found by linear regression of a range of points (Andrews et al.,  
 124 2015; Rugenstein, Caldeira, & Knutti, 2016; Ceppi & Gregory, 2019).

125 Armour et al. (2013) suggested a similar decomposition, but interpreted the com-  
 126 ponents as locally constant feedbacks multiplied by local temperatures with different time  
 127 evolution. However, recent studies suggest that non-local feedbacks are also important  
 128 (Andrews et al., 2015; Zhou et al., 2016; Dong et al., 2019; Bloch-Johnson, Rugenstein,

129 & Abbot, 2020), meaning that temperature changes in one region, and in particular the  
 130 West Pacific, can influence feedbacks globally.

131 **2.1 Linear model and response**

A simple model of temperature changes in the climate system can be constructed by considering different boxes or components that store and exchange energy. If assuming that all anomalous heat fluxes are linearly related to temperature anomalies in the system, the heat uptake in all boxes can be written into a linear non-homogeneous system

$$\mathbf{C} \frac{d\mathbf{T}(t)}{dt} = \mathbf{K}\mathbf{T}(t) + \mathbf{F}(t) \quad (6)$$

132 By choosing the vector of temperature change components  $\mathbf{T}$  to be  $K$ -dimensional,  
 133 the system describes  $K$  components that will respond on  $K$  different time scales, and  
 134 the vector  $\mathbf{F}$  the atmospheric forcing acting directly on each component. The heat capacities  
 135 associated with each component are along the diagonal of the diagonal  $K \times K$   
 136 matrix  $\mathbf{C}$ , and coefficients for heat exchange between components and heat loss to the  
 137 atmosphere constitute the matrix  $\mathbf{K}$ . The left-hand side of this equation describes the  
 138 heat uptake of each component, and the sum of all heat uptakes must equal the net radiative  
 139 imbalance  $N$ . In this sum of all components, all fluxes between components cancel  
 140 out, and the sum reduces to Eq. (4).

141 Linear systems like this have been widely studied, often using one, two or three boxes  
 142 (e.g. Geoffroy, Saint-Martin, Olivié, et al., 2013; Fredriksen & Rypdal, 2017). Symmetric  
 143 matrices  $\mathbf{K}$  will describe diffusive heat fluxes depending on the temperature difference  
 144 between two boxes, and feedback parameters will appear on its diagonal. Non-symmetric  
 145 parts may be due to the dependence of temperature anomalies in one box only. For instance  
 146 change in sinking processes due to temperature anomalies in the North Atlantic  
 147 regarded as one box, may by continuity induce horizontal mass and hence energy fluxes  
 148 from adjacent ocean basins regarded as other boxes, independent of the temperature change  
 149 in these boxes.  $\mathbf{K}$  may also incorporate heat fluxes to the deep ocean if assuming they  
 150 can be modelled as linear functions of temperature components (e.g. Held et al., 2010;  
 151 Geoffroy, Saint-Martin, Olivié, et al., 2013).

By applying the method variation of parameters, it can be shown that the solution to Eq. (6) is:

$$\mathbf{T}(t) = \int_{-\infty}^t e^{(t-s)\mathbf{C}^{-1}\mathbf{K}} \mathbf{C}^{-1} \mathbf{F}(s) ds, \quad (7)$$

showing that the temperature at time  $t$  is a response to the forcing experienced at all previous times  $s$ . If the matrix  $\mathbf{C}^{-1}\mathbf{K}$  has only negative eigenvalues,  $-1/\tau_n$ , the solution for each temperature component  $T_k(t)$  will be a weighted sum of  $K$  exponential responses to the global average forcing  $F$  with time scales  $\tau_n$  (where the weights  $\beta_n$  are determined by eigenvalues, eigenvectors, and heat capacities),

$$T_k(t) = \int_{-\infty}^t \sum_{n=1}^K \beta_n e^{(s-t)/\tau_n} F(s) ds \quad (8)$$

Furthermore, the global surface temperature is a weighted average of the components  $T_k(t)$ :

$$\overline{T}(t) = \sum_{n=1}^K c_n \int_{-\infty}^t e^{(s-t)/\tau_n} F(s) ds \quad (9)$$

152 where we define the new weights  $c_n$  to be an area-weighted average of the weights  $\beta_n$ .  
 153 The vector  $\mathbf{F}$  could in principle contain different forcings in different regions. If so, Eq.  
 154 (9) is still valid if the regional forcings are scaled versions of the global average forcing.

155 We recognize Eq. (9) as a convolution between a Green’s function  $G(t)$  and a forcing  $F(t)$ ,  
 156 consistent with Eq. (3):  $T(t) = G(t)*F(t) = \int_{-\infty}^t G(t-s)F(s)ds$ , with  $G(t) = \sum_{n=1}^K G_n(t) =$   
 157  $\sum_{n=1}^K c_n \exp(-t/\tau_n)$ , assuming negative eigenvalues.

## 158 2.2 Estimating linear response in abrupt 4xCO<sub>2</sub> experiments

159 To simplify the estimation of parameters of these responses (time scales  $\tau_n$  and am-  
 160 plitudes  $c_n$ ), we start by fixing the time scales, such that  $T$  and  $N$  depend linearly on  
 161 the remaining parameters  $c_n$ . We find that the exact choice of time scales is not impor-  
 162 tant, as long as we choose them well separated, and within the range of expected time  
 163 scales. Annual time scales are important over land and shallow ocean areas, while decadal  
 164 and centennial time scales are particularly important in ocean regions with deeper mix-  
 165 ing, and hence higher thermal inertia. Following PH17, we use three different time scales.  
 166 They find three time scales to be the smallest number that well describes the temper-  
 167 ature responses. As explained later, we will in addition assume the existence of a fourth  
 168 time scale explaining slower temperature responses than can be observed in the records  
 169 studied in this paper.

170 We analyse data from 21 CMIP5 models, available at [https://esgf-node.llnl](https://esgf-node.llnl.gov/projects/cmip5/)  
 171 [.gov/projects/cmip5/](https://esgf-node.llnl.gov/projects/cmip5/). The variables used are global annual averages of surface air tem-  
 172 peratures (tas), and net top-of-atmosphere radiation, computed as the difference between  
 173 incoming shortwave radiation and outgoing longwave and shortwave radiation (rsdt - rlut  
 174 - rsut). To minimize the effect of possible drifts, the temperature  $T(t)$  and the variables  
 175 used to compute the net top of atmosphere radiation  $N(t)$  time series are defined as de-  
 176 viations from linear trends in the corresponding time period of the control run (trend  
 177 values for the abrupt4xCO<sub>2</sub> period are given in Table S1, and are very small). With this  
 178 definition we also avoid non-zero means of  $N(t)$  in equilibrium, which is the case for many  
 179 models (Forster et al., 2013).

180 The shortest time scale  $\tau_1$  is chosen to be a random number between 1 and 6 years,  
 181 the second time scale  $\tau_2$  is a random factor between 5 and 10 multiplied by  $\tau_1$ , and the  
 182 third is a randomly chosen time scale between 80 and 1000 years. The random choice  
 183 is done 1000 times for each model, and finally, for each model, we keep the set of  $\tau_n$  with  
 184 the best fit to the modelled temperature evolution for 150 years after an abrupt quadru-  
 185 pling of CO<sub>2</sub>. The resulting parameters are dependent on the length of the time series  
 186 used. If using longer time series the longest time-scale responses may change the most,  
 187 but these are also the least important for our 21st century analyses.

The temperature response for these step-forcing experiments can be found by com-  
 puting the integrals in Eq. (9) with a constant forcing  $F_{4xCO_2}$  for  $t > 0$ . This integral  
 results in

$$T_{4xCO_2}(t) = \sum_{n=1}^K a_n(1 - e^{-t/\tau_n}) \quad (10)$$

188 where  $a_n = c_n \tau_n F_{4xCO_2}$  is the equilibrium temperature of each component, and the equi-  
 189 librium climate sensitivity (ECS) is defined as  $\frac{1}{2} \sum_{n=1}^K a_n$  (equilibrium response to a dou-  
 190 bling of CO<sub>2</sub>).

191 The expression for  $N$  is derived as:

$$\begin{aligned}
 N_{4\times\text{CO}_2}(t) &= F_{4\times\text{CO}_2} + \sum_{n=1}^K (\lambda_n T_n(t)) \\
 &= F_{4\times\text{CO}_2} + \sum_{n=1}^K \left( \lambda_n a_n (1 - e^{-t/\tau_n}) \right) \\
 &= F_{4\times\text{CO}_2} + \sum_{n=1}^K \lambda_n a_n - \sum_{n=1}^K \lambda_n a_n e^{-t/\tau_n} \\
 &= - \sum_{n=1}^K \lambda_n a_n e^{-t/\tau_n}
 \end{aligned}$$

192 where we in the last step set that  $F_{4\times\text{CO}_2} + \sum_{n=1}^K \lambda_n a_n = 0$ , due to the constraint that  
 193  $N \rightarrow 0$  when  $t \rightarrow \infty$ . Introducing the notation that  $b_n = -a_n \lambda_n$  gives us  $N_{4\times\text{CO}_2}(t) =$   
 194  $\sum_{n=1}^K N_n(t) = \sum_{n=1}^K b_n e^{-t/\tau_n}$ , and  $F_{4\times\text{CO}_2} = -\sum_{n=1}^K \lambda_n a_n = \sum_{n=1}^K b_n$ .

195 The parameters  $a_n, b_n$  could be found using linear regression, but that does some-  
 196 times violate the physical assumption that these should have the same sign as the forc-  
 197 ing. Therefore we have used the non-negative least squares algorithm to ensure positive  
 198 parameters. This is used only for finding  $a_n$ , and the resulting temperature responses  
 199 are shown in Figure 1 b). This method could also have been used to find  $b_n$ , but this does  
 200 not seem to provide a sufficiently good fit on the short scales. Instead,  $\lambda_n$  are determined  
 201 in a Gregory plot, and then used to compute  $b_n = -\lambda_n a_n$ .

### 202 2.3 Algorithm for estimating $\lambda_n$

203 The  $\lambda_n, n = 1, \dots, K$  are all determined from linear fits in a Gregory plot, as  
 204 shown in Figure 1 a). We start with estimating  $\lambda_3$  corresponding to time scale  $\tau_3$ , then  
 205 we estimate  $\lambda_2$ , and finally  $\lambda_1$ . We assume that the sum  $\sum_{n=1}^3 a_n$  underestimates the  
 206 equilibrium response, since the sum excludes the response on the multi-millennial scale  
 207  $\tau_4$ . We assume  $\tau_4$  is so large, that we can make the following approximations for  $t \leq$   
 208 150 years:

$$T_4(t) = a_4 \left( 1 - e^{-t/\tau_4} \right) \approx 0 \quad (11)$$

$$N_4(t) = b_4 e^{-t/\tau_4} \approx b_4 \quad (12)$$

209 Hence  $T(t) \approx \sum_{n=1}^3 T_n(t)$  and  $N(t) \approx b_4 + \sum_{n=1}^3 N_n(t)$ , where  $b_4$  could be interpreted  
 210 as a constant heat flux going into the deeper oceans, not leading to more surface warm-  
 211 ing on short scales. We made the somewhat arbitrary choice of setting  $\tau_4 = 5000$  years,  
 212 and assume  $\lambda_4 = \lambda_3$ . The results are not sensitive to the choice of  $\tau_4$  as long as the ap-  
 213 proximations in Eqs. (11) and (12) are fair. In the 150 year long runs considered in this  
 214 paper we have no information about  $\lambda_4$ , but longer runs show that the feedback param-  
 215 eter changes little on the longer time scales (Rugenstein et al., 2020).

216 **Determining  $\lambda_3$ :** We consider only temperatures larger than the equilibrium tem-  
 217 perature of the first two components, such that  $T_1(t) + T_2(t) \approx a_1 + a_2$ , and we have:  
 218  $N(t) \approx -\lambda_3(a_3 - T_3(t)) + b_4$ . The total temperature is therefore approximated by  $T(t) \approx$   
 219  $a_1 + a_2 + T_3(t)$ , resulting in  $N(t) \approx -\lambda_3(a_1 + a_2 + a_3 - T(t)) + b_4$ . This shows that  $N$  is  
 220 approximately a linear function of  $T$  with slope  $\lambda_3$  for  $T > a_1 + a_2$ . Therefore,  $\lambda_3$  is  
 221 computed by linear regression of these points, and the equilibrium temperature found  
 222 by following this line until  $N = 0$ . This equilibrium estimate should be a higher esti-  
 223 mate than  $\sum_{n=1}^3 a_n$ , and the difference we recognize as  $a_4$ . Whenever the unphysical re-  
 224 sult  $a_4 < 0$  is obtained (at least according to our assumed model), we exclude the cho-  
 225 sen time scales from our analysis.  $b_4$  is computed as  $b_4 = -\lambda_3 a_4$ .

**Determining  $\lambda_2$ :** First we subtract our estimates of  $T_3(t)$ ,  $T_4(t)$  and  $N_3(t)$ ,  $N_4(t)$  from the time series  $T(t)$  and  $N(t)$ , respectively. We then obtain estimates of  $T_1(t) + T_2(t)$  and  $N_1(t) + N_2(t)$ , and these points are the gray dots in Figure 1a). For  $a_1 < T_1(t) + T_2(t) < a_1 + a_2$ ,  $T_1(t) + T_2(t)$  is approximately  $a_1 + T_2(t)$ , and should equal the equilibrium value  $a_1 + a_2$  when  $N_1(t) + N_2(t) = 0$ . In this range,  $N_1(t) + N_2(t) \approx -\lambda_2(a_2 - T_2(t))$ , approximately linearly related to  $T_1(t) + T_2(t)$ . Therefore,  $\lambda_2$  is estimated using a least-squares algorithm forcing the linear fit to go through the point  $(a_1 + a_2, 0)$ .

**Determining  $\lambda_1$ :** We subtract estimates of  $(T_2(t), N_2(t))$  from the gray dots to obtain estimates of  $T_1(t)$  and  $N_1(t)$  (light gray dots in Figure 1). We have now that  $N_1(t) \approx -\lambda_1(a_1 - T_1(t))$ , and we can as previously use least squares to compute  $\lambda_1$ , forcing the linear fit to pass the point  $(a_1, 0)$ .

In the least squares fits, we also include an upper time limit to the set of points to be included in the calculation. This limit is set to the first time step after reaching 99% of the equilibrium temperature of the component of interest. In this way, our slope is associated with the response on the particular time scale  $\tau_n$ , and little influenced by the fluctuations around the equilibrium values. Changing this limit to e.g. 90% or 95% has only minor effects on the results. Feedback parameters associated with fluctuations around the base state, or more precisely, radiative restoring coefficients are studied in several papers (Colman & Power, 2010; Colman & Hanson, 2013; Lutsko & Takahashi, 2018; Bloch-Johnson, Rugenstein, & Abbot, 2020). Depending on the model, they can be similar or different from those associated with the final fluctuation after a quadrupling of  $\text{CO}_2$  (Rugenstein et al., 2020), and they may also differ from feedbacks associated with forced responses (e.g. Zhou et al., 2015; Dessler & Forster, 2018).

## 2.4 New estimates of effective forcing

Using our parameter estimates from the previous subsections, we can for any experiment compute a new estimate of the effective forcing as follows:

1. Compute  $F(t)$  using F13's method (a single estimate of  $\lambda$ ), and take this as the initial estimate of the effective forcing.
2. Use this forcing estimate and amplitudes  $c_n = \frac{a_n}{\tau_n F_{4\times\text{CO}_2}}$  estimated from  $4\times\text{CO}_2$  experiments to compute the components  $T_n(t)$  from Eq. (3) by performing convolution integrals.
3. A new estimate of  $F(t)$  can then be computed as:

$$F(t) = N(t) - \sum_n \lambda_n T_n(t) \quad (13)$$

4. Repeat steps 2-3 until convergence of  $F(t)$ .

We demonstrate how the method can be applied to study the forcing for the historical period and the four representative concentration pathways (RCPs) RCP2.6, RCP4.5, RCP6.0 and RCP8.5.

## 3 Results

The results of the linear response fit for  $T(t)$  and  $N(t)$  following an abrupt quadrupling of  $\text{CO}_2$  are given for the model NorESM1-M in Figure 1, and the estimated parameters are listed in Table 1. We note from Figure 1a) that both the forcing and equilibrium temperature estimates are higher than when obtained from a straight line fit. The narrow spread of the light blue lines also indicate that the choice of time scales is of little importance, and hence not affecting the overall conclusions. Similar plots are shown for the other models listed in Table 1 in the Supporting information. The uncertainty in both the forcing estimate and ECS estimate vary substantially from model to

**Table 1.** Estimated parameters, where we define  $F_{2x}$  and  $T_{2x}$  to be half the forcing and equilibrium temperature estimated for a quadrupling of  $\text{CO}_2$ . The parameters in parentheses  $(-\lambda)$ ,  $(F_{2x})$  and  $(T_{2x})$  are estimated from a single linear regression over years 1-150 in a Gregory plot. The results differ slightly from the numbers reported from the Gregory method by Andrews et al. (2012), possibly because of minor differences in the way global annual average values are constructed. For one model (GFDL-ESM2G) the best fit consists of two exponential responses, where we estimate  $a_2 = 0$  and report  $\lambda_2 = b_2/a_2$  as 'NaN'.

	$\tau_1$	$\tau_2$	$\tau_3$	$-\lambda_1$	$-\lambda_2$	$-\lambda_3$	$(-\lambda)$	$F_{2x}$	$(F_{2x})$	$T_{2x}$	$(T_{2x})$
ACCESS1-0	2.43	12.79	231.10	1.30	1.12	0.56	0.78	3.72	2.97	4.33	3.83
ACCESS1-3	1.13	5.80	150.10	1.46	1.30	0.56	0.82	3.60	2.89	4.12	3.53
CanESM2	2.86	26.39	279.11	1.30	1.01	0.91	1.04	4.24	3.83	3.83	3.69
CCSM4	1.04	5.52	197.28	1.32	1.77	0.90	1.18	4.02	3.47	3.19	2.94
CNRM-CM5	1.45	10.71	392.15	1.38	1.09	1.22	1.14	3.87	3.71	3.20	3.25
CSIRO-Mk3-6-0	1.62	11.29	308.98	1.86	1.12	0.41	0.63	3.94	2.58	4.94	4.08
GFDL-CM3	3.28	32.58	98.81	1.21	0.80	0.63	0.75	3.61	2.99	4.24	3.97
GFDL-ESM2G	2.98	17.50	291.97	1.76	NaN	0.90	1.29	3.65	3.09	2.67	2.39
GFDL-ESM2M	1.03	5.77	240.02	1.52	1.58	1.22	1.38	3.58	3.36	2.52	2.44
GISS-E2-H	1.56	10.43	186.27	2.02	1.83	1.40	1.65	4.21	3.81	2.39	2.31
GISS-E2-R	1.51	10.61	232.40	2.98	1.02	1.42	1.79	5.09	3.78	2.25	2.11
HadGEM2-ES	1.01	8.39	367.62	1.96	0.89	0.35	0.63	4.02	2.90	5.91	4.61
inmcm4	1.02	5.65	597.43	1.90	1.48	1.28	1.43	3.18	2.98	2.14	2.08
IPSL-CM5A-LR	1.72	16.54	163.83	1.03	0.84	0.58	0.75	3.43	3.10	4.55	4.13
IPSL-CM5B-LR	1.21	8.01	80.30	2.39	1.11	0.91	1.02	3.64	2.64	2.68	2.60
MIROC-ESM	1.78	11.32	266.35	1.96	0.92	0.68	0.91	5.37	4.26	5.21	4.67
MIROC5	2.77	15.17	89.28	1.72	1.43	1.36	1.52	4.38	4.13	2.80	2.72
MPI-ESM-LR	1.81	9.20	202.56	1.30	1.50	0.86	1.13	4.53	4.09	3.91	3.63
MPI-ESM-MR	1.02	6.23	158.54	2.27	1.45	0.94	1.18	5.15	4.07	3.67	3.46
MRI-CGCM3	1.42	11.61	233.73	2.22	1.34	0.96	1.25	4.05	3.24	2.76	2.60
NorESM1-M	1.75	9.34	273.12	1.87	1.52	0.78	1.11	3.88	3.10	3.17	2.80

270 model. Models with a rapid initial warming, like GISS-E2-R, have fewer points constrain-  
 271 ing the regression estimate for the shortest time scale, implying larger uncertainty of the  
 272 forcing.

273 An overview of all our estimates of the  $4x\text{CO}_2$  forcing are also presented in Fig-  
 274 ure 2. In addition, we compare our forcing estimates to regression estimates done for years  
 275 1-20 and years 1-150. In all except one model, the 1-20 year regression gives a higher es-  
 276 timate than the 1-150 year regression. And in all but two models, our best forcing es-  
 277 timate is even higher than estimates obtained from regression of years 1-20.

278 Using global annual means of  $N(t)$  and  $T(t)$  from the coupled models for the his-  
 279 torical and RCP experiments, we apply the algorithm described in Section 2.4 to com-  
 280 pute forcing estimates for the time period 1850 - 2100. Our new forcing estimate for the  
 281 historical and RCP8.5 experiment for NorESM1-M diverges from the forcing estimate  
 282 using a single feedback parameter when approaching the end of the 21st century (Fig-  
 283 ure 3a). The difference is about  $2 \text{ W/m}^2$  in 2100, and only smaller differences are seen  
 284 during the historical period. As a result, the sum of the linear responses we compute by  
 285 convolving with the two forcing estimates according to Eq. (3) also diverge (dashed curves  
 286 in Figure 3b), reaching a difference of almost 1 degree in year 2100. We note that the  
 287 linear response to our new forcing (dashed blue curve) is remarkably close to the climate

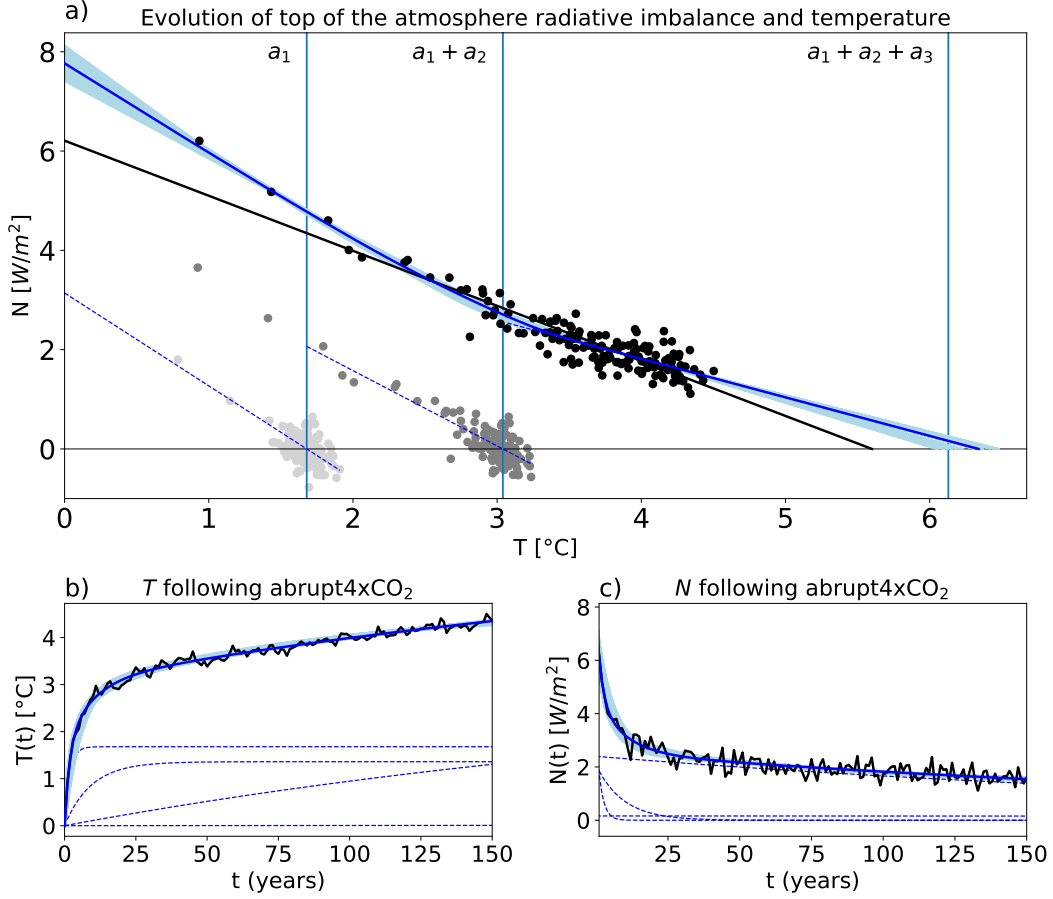


**Figure 1.** Results for NorESM1-M: a) The black dots and line is a conventional Gregory plot, the light blue lines are our fits to the black points with 1000 different choices of time scales, and the dark blue fit is when using the best fits for the temperature in b). Vertical blue lines are the sums of equilibrium temperatures  $\sum_{n=1}^m a_n$ ,  $m = 1, 2, 3$ . The gray dots are  $N$  vs.  $T$  after subtracting components associated with the longer time scales, and the dashed blue lines are fits to these dots. b) The black curve is the climate model temperature output, and the light blue curves are best fits to the modelled temperature using 1000 different choices of time scales. The dark blue curve is the best fit, and the dashed blue curves are the individual components due to the four time scales summed over to obtain this fit. c) As panel b), but for the change in net top of the atmosphere radiation.

288 model temperature output, indicating that our alternative forcing definition and linear  
 289 response assumption is a good approximation for this model.

290 By computing the time-varying feedback parameter  $\lambda(t)$  using Eq. (5), we find a  
 291 generally higher magnitude than the single estimate of  $\lambda$ . During the historical period  
 292 the global temperature response is often close to 0, causing high fluctuations in the es-  
 293 timated  $\lambda(t)$ . The estimate becomes more stable for the future scenarios, where we find  
 294 a slowly decreasing magnitude of  $\lambda(t)$ , consistent with a higher weighting of the slow re-  
 295 sponses. For all years in the experiment, the magnitude of  $\lambda(t)$  is still considerably higher  
 296 than the single regression estimate, hence the term  $-\lambda(t)T(t)$  gives a higher contribu-  
 297 tion to the forcing estimate. This effect on the forcing is however only visible when the  
 298 temperature response is strong.

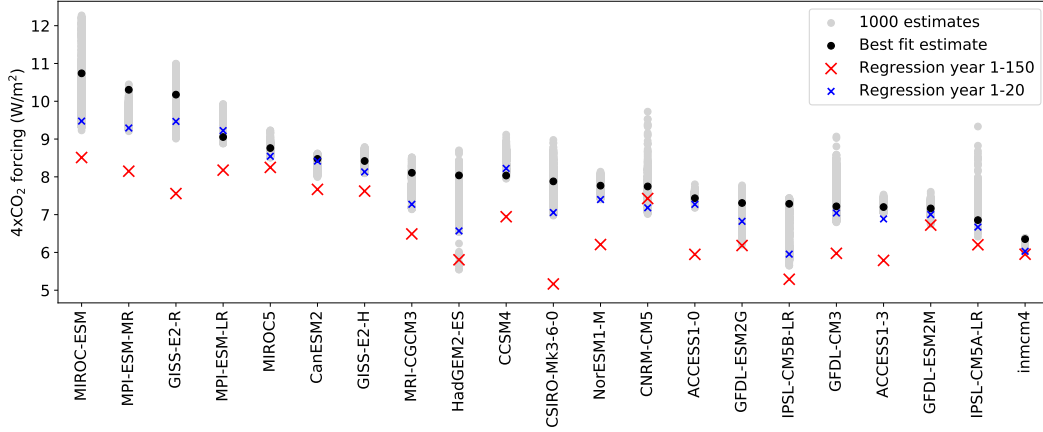


**Figure 2.** A summary of the  $4xCO_2$  forcing estimates made in this paper, to provide an overview of their uncertainties and how they compare to regression estimates.

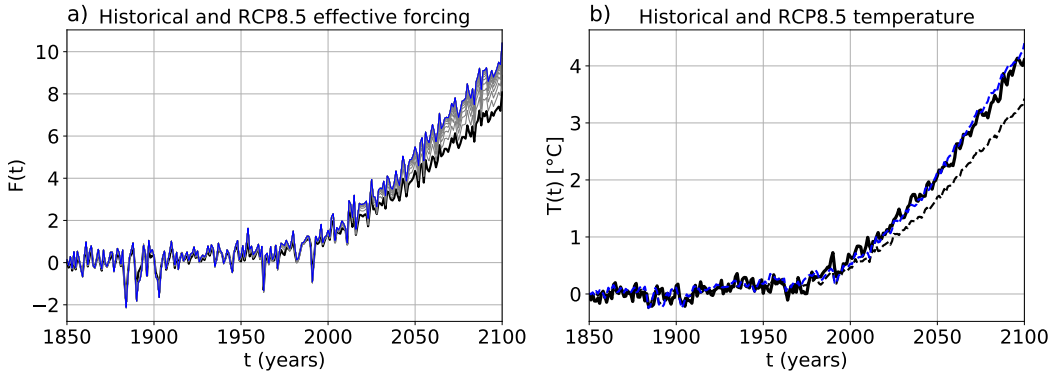


**Figure 3.** Results for NorESM1-M: a) The black curve is the forcing computed as in F13, using a single and constant value of  $\lambda$ . The gray curves are the iterations of the algorithm described in section 2.4, using three different  $\lambda$ 's, and the blue curve the new forcing we have converged to after 20 iterations. b) The thick black curve is the modelled temperature change, and the black and blue dashed curves the linear responses to the black and blue curves in a), applying the same response function as estimated in Figure 1 b).

299 Repeating the analysis in Figure 3 for all models and scenarios shows that the method  
 300 presented here works well for many models, but not all (Figures in supporting informa-  
 301 tion). A summary of these results are given in Figure 4, where panel a) compares the  
 302 mean estimated forcing over years 2091-2100 using the two different methods. The names  
 303 of the scenarios are constructed to reflect the intended forcing in the end of the 21st  
 304 century, and these forcing levels are also shown for comparison. We find that model esti-  
 305 mates using F13's method are centered at lower values, while our new forcing estimates  
 306 are centered close to or slightly above the intended levels. However, the intended forc-  
 307 ing is difficult to prescribe as it depends on model-specific fast adjustments, so we can  
 308 only expect these to be approximate values. The GISS-E2-R model might be considered  
 309 as an outlier, and its response to abrupt $4xCO_2$  is also visually different from the other  
 310 models.

311 Consistent with the increase in forcing level, we observe an increase in the estimated  
 312 linear temperature responses in panel b). The linear responses to F13 forcing are mostly

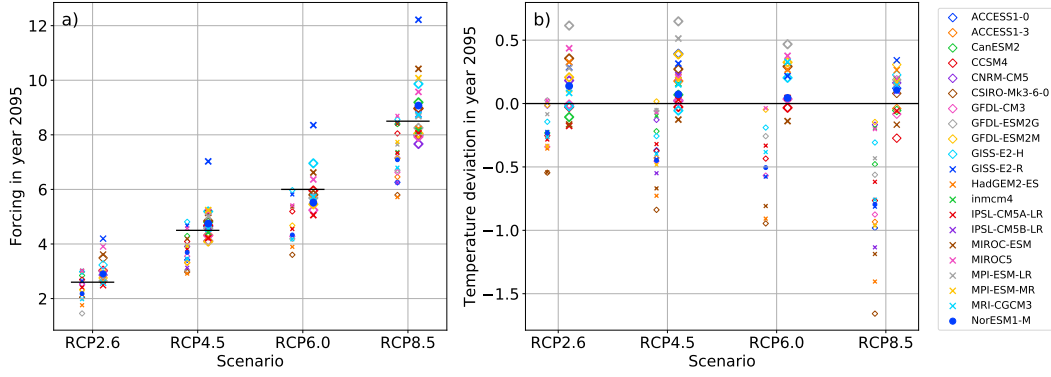


**Figure 4.** Estimated forcing (a) and temperature difference between the result of the linear response and the climate model output (b). For each scenario, the left points show results using F13’s method, and the right points show results using our method. Values in year 2095 are computed by averaging over the ten years 2091-2100. The forcing levels 2.6, 4.5, 6.0 and 8.5  $\text{W/m}^2$  are also shown for reference in a) as horizontal black lines.

313 lower than the climate model temperature output, and the responses to our new forcing  
 314 are scattered around, with a center slightly above. Some deviation from the climate  
 315 model temperature is expected due to internal variability, and to assess this expected  
 316 uncertainty, we refer to the model spread of the Community Earth System Model Large  
 317 Ensemble (CESM-LE) (Kay et al., 2015). Here 40 model simulations for the historical  
 318 + RCP8.5 scenarios from the same model show a model spread of around 0.4 K, which  
 319 is attributed to internal variability.

320 Using F13 forcing, the linear response is within these uncertainties for only a few  
 321 models. For the new forcing, more models are within this uncertainty range than out-  
 322 side. There are also other uncertainties to consider, e.g. associated with our parameter  
 323 estimation method, probably making the expected uncertainty interval larger than 0.4  
 324 K. The uncertainty due to internal variability is also model-dependent (Olonscheck et  
 325 al., 2020), hence it is difficult to identify models where our linear response hypothesis  
 326 and forcing estimation method fail.

327 We note also that the uncertainty of the future scenario forcing estimates is strongly  
 328 related to the uncertainty of the  $4x\text{CO}_2$  forcing estimates, since both are highly influ-  
 329 enced by  $\lambda_1$ . This is particularly apparent for the GISS-E2-R model, where the response  
 330 of the first few years is so abrupt that forcing estimates, and hence linear responses, are  
 331 uncertain with both our and F13’s estimation method.

332 In the two models CNRM-CM5 and MIROC5 the two forcing estimates are very  
 333 similar, because the feedback is close to constant for all years. For these models we find  
 334 also that the forcing estimate based on a single feedback parameter gives a slightly bet-  
 335 ter estimate of the linear response. So if the global feedback in fact is constant for all  
 336 years, using all years in the regression should give a more certain estimate of the feed-  
 337 back parameter, and therefore also more certain forcing estimates.

338 For the three models GFDL-ESM2G, GFDL-ESM2M, and Inmcm4 we find that  
 339 our method is performing less well (see Figures in the Supporting information). The rea-  
 340 son is probably linked to the almost constant  $4x\text{CO}_2$  temperature responses over years  
 341  $\sim 20 - 70$ ,  $\sim 20 - 60$  and  $\sim 20 - 120$ , respectively. Our linear response with exponen-  
 342 tially relaxing temperatures always predicts continuously increasing temperatures, which  
 343 therefore poorly approximates these  $4x\text{CO}_2$  global temperatures. The flattening of the

344 response could possibly be linked to changes in the ocean circulation, e.g. a slowdown  
 345 of the Atlantic meridional overturning circulation. In that case, linear systems with com-  
 346 plex eigenvalues giving oscillatory responses could be an alternative solution. Hence, we  
 347 will not disregard linear response in these results, but leave further testing of including  
 348 oscillations in the responses to future studies.

## 349 4 Discussion

350 For most abrupt4xCO<sub>2</sub> experiments the Gregory plot follows a convex curve, hence  
 351 our forcing estimates are mostly higher than those found from simple regression anal-  
 352 yses over 150 years (Andrews et al., 2012), or using only the first 20 years (Andrews et  
 353 al., 2015; Larson & Portmann, 2016). As suggested by PH17, this convexity could be ex-  
 354 plained by considering different feedback parameters associated with the different time  
 355 scales of the responses. The time-scale dependence of the feedback parameter could be  
 356 physically explained simply as feedbacks varying in strength at different time scales, or  
 357 it could be regionally different feedbacks weighted differently with time in the global av-  
 358 erage when the pattern of surface warming evolves. Since it is likely a combination of  
 359 these explanations, an interpretation of our parameters could be summarized into:  $\lambda_1$ :  
 360 Average of annual-scale feedbacks in regions with strong annual-scale responses,  $\lambda_2$ : Av-  
 361 erage of decadal-scale feedbacks in regions with strong decadal-scale responses,  $\lambda_3$ : Av-  
 362 erage of centennial-scale feedbacks in regions with strong centennial-scale responses.

363 The theory described in this paper does not include an explicit temperature-dependence  
 364 of the feedback parameter (Rohrschneider et al., 2019; Bloch-Johnson, Rugenstein, Stolpe,  
 365 et al., 2020), since it is assumed that Eq. (6) is linear and  $\mathbf{K}$  is independent of temper-  
 366 ature. However, our estimation algorithm does not clearly distinguish between a time-  
 367 scale dependence and a temperature-dependence of the feedbacks, since these dependen-  
 368 cies are intrinsically linked. In particular, the strong temperature responses to 4xCO<sub>2</sub>  
 369 is invoked on the long time scales, where the responses to the shorter time scales have  
 370 already been realised, hereby affecting the feedback parameters if they have tempera-  
 371 ture dependence. If the 4xCO<sub>2</sub> responses have temperature-dependent feedbacks, the model  
 372 needed to explicitly explain them becomes nonlinear, and our linear approach may per-  
 373 form less well in providing responses to other scenarios with weaker or stronger temper-  
 374 ature responses than that of 4xCO<sub>2</sub>. We believe this only causes smaller errors in the  
 375 temperature responses studied here, but it is a potential explanation for our forcing and  
 376 responses for the future scenarios being slightly overestimated.

377 The fixed-SST 4xCO<sub>2</sub> forcing estimates reported by Andrews et al. (2012) are also  
 378 higher than regression-based estimates over 150 years, and our estimated forcing is even  
 379 higher than the fixed-SST forcing. One reason for this difference is that fixed-SST es-  
 380 timates let atmospheric and land surface temperatures increase before the radiative im-  
 381 balance is diagnosed. Hence this estimate is more comparable to our radiative imbalance  
 382 after some months of adjustments of  $T(t)$  and  $N(t)$ . Tang et al. (2019) finds that the  
 383 fixed-SST forcing is lower than the regression estimate for some models. An important  
 384 advantage of fixed-SST estimates compared to regression-based estimates is the reduced  
 385 level of noise (Forster et al., 2016). This noise reduction is important when estimating  
 386 time-evolving forcing using prescribed-SST methods (Forster et al., 2013). Regression-  
 387 based estimates are influenced by changes in  $T(t)$  arising due to internal variability, e.g.  
 388 El Niño events, which could drive changes in  $N(t)$ . In prescribed-SST methods the temperature-  
 389 driven changes in  $N(t)$  is subtracted.

390 Linear response theory is widely used to describe responses of climate variables.  
 391 If a forcing record is known, linear response is a computationally cheap tool to estimate  
 392 e.g. temperature responses compared to running a fully coupled climate model. Many  
 393 studies assume a Green’s function taking a certain form, with unknown parameters that  
 394 need to be estimated. For box models taking the form of Eq. (6) the Green’s function

395 is a sum of exponential functions, but power-laws with fewer parameters have also been  
 396 used with success (Rypdal & Rypdal, 2014; Fredriksen & Rypdal, 2017). Linear responses  
 397 to RCP forcing are often studied using a non-parametric approach developed by Good  
 398 et al. (2011). This method was used in Good et al. (2013) to find the response to RCP  
 399 scenarios using the forcing computed by F13. They use this to simulate only differences  
 400 between RCP scenarios, while we attempt to simulate the full temperature evolution since  
 401 the historical runs started until year 2100. Another difference to our approach is that  
 402 we obtain a smoother estimate of the expected response to forcing, with fluctuations only  
 403 coming from the forcing, while the responses of Good et al. (2013) are themselves influ-  
 404 enced by internal variability.

## 405 5 Conclusions

406 The method presented here suggests a clean separation between forcing and responses  
 407 to forcing, where the estimated parameters from abrupt4xCO<sub>2</sub> experiments are used to  
 408 determine forcing and surface temperature responses for other experiments. The result-  
 409 ing RCP forcing estimates at the end of the 21st century is closer to the target levels than  
 410 previous estimates by F13. Our high forcing estimates are strongly influenced by the high  
 411 magnitude of the feedback parameter  $\lambda_1$  at annual time scales. Unfortunately this value  
 412 is uncertain, as it depends crucially on the first few years of adjustment. Using more en-  
 413 semble members of abrupt4xCO<sub>2</sub> experiments may help constrain the estimate of  $\lambda_1$  (Rugenstein,  
 414 Gregory, et al., 2016).

415 Forcing based on fixed-SST methods is often higher than the regression estimate  
 416 over 150 years (Andrews et al., 2012; Tang et al., 2019), has a smaller uncertainty and  
 417 is more computationally efficient (Forster et al., 2016). However, these forcing estimates  
 418 are only available for a few models and scenarios in CMIP5. They will be available for  
 419 more models and scenarios in CMIP6 (Smith et al., 2020), but far from all. The forc-  
 420 ing estimation method presented here could therefore be a valuable supplement in the  
 421 cases where fixed-SST forcing is unknown, particularly for models where a linear rela-  
 422 tion between  $N$  and  $T$  is a poor approximation. Improved forcing estimates could help  
 423 to quantify the dependency of forcing value on CO<sub>2</sub> concentration in studies compar-  
 424 ing e.g. 0.5x, 2x, 4x, 8x CO<sub>2</sub>, and temperature dependence of feedbacks (Bloch-Johnson,  
 425 Rugenstein, Stolpe, et al., 2020).

426 Putting forcing, linear responses, and nonconstancy of the global feedback param-  
 427 eter into a unified framework provides also an important insight into why the traditional  
 428 regression-based forcing estimates may be too low. Furthermore, it suggests how these  
 429 methods can be improved to provide better forcing estimates, resolving the problems caused  
 430 by assuming a constant feedback parameter in regression-based methods (Forster et al.,  
 431 2016).

## 432 Acknowledgments

433 The CMIP5 data are available at <https://esgf-node.llnl.gov/projects/cmip5/>. The  
 434 forcing estimates from this paper will be stored in <https://dataverse.no/>, and can be  
 435 accessed through <https://doi.org/10.18710/IHUVTB>.

## 436 References

- 437 Andrews, T., Gregory, J. M., & Webb, M. J. (2015). The Dependence of Ra-  
 438 diative Forcing and Feedback on Evolving Patterns of Surface Tempera-  
 439 ture Change in Climate Models. *Journal of Climate*, 28(4), 1630–1648.  
 440 <https://doi.org/10.1175/JCLI-D-14-00545.1>  
 441 Andrews, T., Gregory, J. M., Webb, M. J., & Taylor, K. E. (2012). Forc-  
 442 ing, feedbacks and climate sensitivity in CMIP5 coupled atmosphere-

- ocean climate models. *Geophysical Research Letters*, *39*, L09712.  
<https://doi.org/10.1029/2012GL051607>
- Andrews, T., & Webb, M. J. (2018). The Dependence of Global Cloud and Lapse Rate Feedbacks on the Spatial Structure of Tropical Pacific Warming. *Journal of Climate*, *31*(2), 641-654. <https://doi.org/10.1175/JCLI-D-17-0087.1>
- Armour, K. C. (2017). Energy budget constraints on climate sensitivity in light of inconstant climate feedbacks. *Nature Climate Change*, *7*, 331 – 335. <https://doi.org/10.1038/nclimate3278>
- Armour, K. C., Bitz, C. M., & Roe, G. H. (2013). Time-Varying Climate Sensitivity from Regional Feedbacks. *Journal of Climate*, *26*, 4518–4534. <https://doi.org/10.1175/JCLI-D-12-00544.1>
- Bacmeister, J. T., Hannay, C., Medeiros, B., Gettelman, A., Neale, R., Fredriksen, H. B., ... Otto-Bliesner, B. (2020). CO2 increase experiments using the Community Earth System Model (CESM): Relationship to climate sensitivity and comparison of CESM1 to CESM2. *Journal of Advances in Modeling Earth Systems*, *12*, e2020MS002120. <https://doi.org/10.1029/2020MS002120>
- Bloch-Johnson, J., Rugenstein, M., & Abbot, D. S. (2020). Spatial radiative feedbacks from internal variability using multiple regression. *Journal of Climate*, *33*, 4121–4140. <https://doi.org/10.1175/JCLI-D-19-0396.1>
- Bloch-Johnson, J., Rugenstein, M., Stolpe, M. B., Rohrschneider, T., Zheng, Y., & Gregory, J. (2020). Climate sensitivity increases under higher CO<sub>2</sub> levels due to positive feedback temperature dependence. *Submitted to Journal of Geophysical Research*.
- Ceppi, P., & Gregory, J. M. (2017). Relationship of tropospheric stability to climate sensitivity and Earth’s observed radiation budget. *Proceedings of the National Academy of Sciences*, *114*(50), 13126–13131. <https://doi.org/10.1073/pnas.1714308114>
- Ceppi, P., & Gregory, J. M. (2019). A refined model for the Earth’s global energy balance. *Climate Dynamics*, *53*, 4781–4797. <https://doi.org/10.1007/s00382-019-04825-x>
- Chung, E.-S., & Soden, B. J. (2015). An assessment of methods for computing radiative forcing in climate models. *Environmental Research Letters*, *10*(7), 074004. <https://doi.org/10.1088/1748-9326/10/7/074004>
- Colman, R. A., & Hanson, L. I. (2013). On atmospheric radiative feedbacks associated with climate variability and change. *Climate Dynamics*, *40*(1), 475–492. <https://doi.org/10.1007/s00382-012-1391-3>
- Colman, R. A., & Power, S. B. (2010). Atmospheric radiative feedbacks associated with transient climate change and climate variability. *Climate Dynamics*, *34*, 919-933. <https://doi.org/10.1007/s00382-009-0541-8>
- Dessler, A. E. (2020). Potential Problems Measuring Climate Sensitivity from the Historical Record. *Journal of Climate*, *33*(6), 2237-2248. <https://doi.org/10.1175/JCLI-D-19-0476.1>
- Dessler, A. E., & Forster, P. M. (2018). An Estimate of Equilibrium Climate Sensitivity From Interannual Variability. *Journal of Geophysical Research: Atmospheres*, *123*(16), 8634-8645. <https://doi.org/10.1029/2018JD028481>
- Dong, Y., Armour, K. C., Zelinka, M. D., Proistosescu, C., Battisti, D. S., Zhou, C., & Andrews, T. (2020). Intermodel Spread in the Pattern Effect and Its Contribution to Climate Sensitivity in CMIP5 and CMIP6 Models. *Journal of Climate*, *33*(18), 7755-7775. <https://doi.org/10.1175/JCLI-D-19-1011.1>
- Dong, Y., Proistosescu, C., Armour, K. C., & Battisti, D. S. (2019). Attributing Historical and Future Evolution of Radiative Feedbacks to Regional Warming Patterns using a Green’s Function Approach: The Preeminence of the Western Pacific. *Journal of Climate*, *32*(17), 5471-5491. <https://doi.org/10.1175/JCLI-D-18-0843.1>
- Forster, P. M., Andrews, T., Good, P., Gregory, J. M., Jackson, L. S., & Zelinka, M.

- 498 (2013). Evaluating adjusted forcing and model spread for historical and future  
 499 scenarios in the CMIP5 generation of climate models. *Journal of Geophysical*  
 500 *Research*, *118*, 1139–1150. <https://doi.org/10.1002/jgrd.50174>
- 501 Forster, P. M., Richardson, T., Maycock, A. C., Smith, C. J., Samset, B. H., Myhre,  
 502 G., ... Schulz, M. (2016). Recommendations for diagnosing effective radiative  
 503 forcing from climate models for CMIP6. *Journal of Geophysical Research:*  
 504 *Atmospheres*, *121*(20), 12,460–12,475. <https://doi.org/10.1002/2016JD025320>
- 505 Fredriksen, H.-B., & Rypdal, M. (2017). Long-range persistence in global surface  
 506 temperatures explained by linear multibox energy balance models. *Journal of*  
 507 *Climate*, *30*, 7157–7168. <https://doi.org/10.1175/JCLI-D-16-0877.1>
- 508 Geoffroy, O., Saint-Martin, D., Bellon, G., Voldoire, A., Olivié, D., & Tytéca,  
 509 S. (2013). Transient Climate Response in a Two-Layer Energy-Balance  
 510 Model. Part II: Representation of the Efficacy of Deep-Ocean Heat Uptake  
 511 and Validation for CMIP5 AOGCMs. *Journal of Climate*, *26*(6), 1859–1876.  
 512 <https://doi.org/10.1175/JCLI-D-12-00196.1>
- 513 Geoffroy, O., Saint-Martin, D., Olivié, D. J. L., Voldoire, A., Bellon, G., &  
 514 Tytéca, S. (2013). Transient Climate Response in a Two-Layer Energy-  
 515 Balance Model. Part I: Analytical Solution and Parameter Calibration Us-  
 516 ing CMIP5 AOGCM Experiments. *Journal of Climate*, *26*, 1841–1857.  
 517 <https://doi.org/10.1175/JCLI-D-12-00195.1>
- 518 Good, P., Gregory, J. M., & Lowe, J. A. (2011). A step-response simple climate  
 519 model to reconstruct and interpret AOGCM projections. *Geophysical Research*  
 520 *Letters*, *38*, L01703. <https://doi.org/10.1029/2010GL045208>
- 521 Good, P., Gregory, J. M., Lowe, J. A., & Andrews, T. (2013). Abrupt CO<sub>2</sub> ex-  
 522 periments as tools for predicting and understanding CMIP5 representative  
 523 concentration pathway projections. *Climate Dynamics*, *40*(3), 1041–1053.  
 524 <https://doi.org/10.1007/s00382-012-1410-4>
- 525 Gregory, J. M., & Andrews, T. (2016). Variation in climate sensitivity and feedback  
 526 parameters during the historical period. *Geophysical Research Letters*, *43*(8),  
 527 3911–3920. <https://doi.org/10.1002/2016GL068406>
- 528 Gregory, J. M., Ingram, W. J., Palmer, M. A., Jones, G. S., Stott, P. A., Thorpe,  
 529 R. B., ... Williams, K. D. (2004). A new method for diagnosing radiative  
 530 forcing and climate sensitivity. *Geophysical Research Letters*, *31*, L03205.  
 531 <https://doi.org/10.1029/2003GL018747>
- 532 Hansen, J., Sato, M., Ruedy, R., Nazarenko, L., Lacis, A., Schmidt, G. A., ...  
 533 Zhang, S. (2005). Efficacy of climate forcings. *Journal of Geophysical Re-*  
 534 *search: Atmospheres*, *110*(D18). <https://doi.org/10.1029/2005JD005776>
- 535 Held, I., Winton, M., Takahashi, K., Delworth, T. L., Zeng, F., & Vallis, G. (2010).  
 536 Probing the Fast and Slow Components of Global Warming by Returning  
 537 Abruptly to Preindustrial Forcing. *Journal of Climate*, *23*, 2418 – 2427.  
 538 <https://doi.org/10.1175/2009JCLI3466.1>
- 539 Kay, J. E., Deser, C., Phillips, A., Mai, A., Hannay, C., Strand, G., ... Vertenstein,  
 540 M. (2015). The Community Earth System Model (CESM) Large Ensemble  
 541 Project: A Community Resource for Studying Climate Change in the Pres-  
 542 ence of Internal Climate Variability. *Bulletin of the American Meteorological*  
 543 *Society*, *96*(8), 1333-1349. <https://doi.org/10.1175/BAMS-D-13-00255.1>
- 544 Larson, E. J. L., & Portmann, R. W. (2016). A Temporal Kernel Method to Com-  
 545 pute Effective Radiative Forcing in CMIP5 Transient Simulations. *Journal of*  
 546 *Climate*, *29*(4), 1497-1509. <https://doi.org/10.1175/JCLI-D-15-0577.1>
- 547 Loeb, N. G., Wang, H., Allan, R. P., Andrews, T., Armour, K., Cole, J. N. S.,  
 548 ... Wyser, K. (2020). New generation of climate models track  
 549 recent unprecedented changes in earth’s radiation budget observed  
 550 by ceres. *Geophysical Research Letters*, *47*(5), e2019GL086705.  
 551 <https://doi.org/10.1029/2019GL086705>
- 552 Lutsko, N. J., & Takahashi, K. (2018). What Can the Internal Variability of CMIP5

- 553 Models Tell Us about Their Climate Sensitivity? *Journal of Climate*, 31(13),  
554 5051–5069. <https://doi.org/10.1175/JCLI-D-17-0736.1>
- 555 Marvel, K., Pincus, R., Schmidt, G. A., & Miller, R. L. (2018). Internal  
556 Variability and Disequilibrium Confound Estimates of Climate Sensitiv-  
557 ity From Observations. *Geophysical Research Letters*, 45(3), 1595–1601.  
558 <https://doi.org/10.1002/2017GL076468>
- 559 Menzel, M. E., & Merlis, T. M. (2019). Connecting Direct Effects of CO<sub>2</sub> Radiative  
560 Forcing to Ocean Heat Uptake and Circulation. *Journal of Advances in Model-  
561 ing Earth Systems*, 11(7), 2163–2176. <https://doi.org/10.1029/2018MS001544>
- 562 Meraner, K., Mauritsen, T., & Voigt, A. (2013). Robust increase in equilibrium cli-  
563 mate sensitivity under global warming. *Geophysical Research Letters*, 40(22),  
564 5944–5948. <https://doi.org/10.1002/2013GL058118>
- 565 Olonscheck, D., Rugenstein, M., & Marotzke, J. (2020). Broad consis-  
566 tency between observed and simulated trends in sea surface tempera-  
567 ture patterns. *Geophysical Research Letters*, 47(10), e2019GL086773.  
568 <https://doi.org/10.1029/2019GL086773>
- 569 Paynter, D., & Frölicher, T. L. (2015). Sensitivity of radiative forcing, ocean heat  
570 uptake, and climate feedback to changes in anthropogenic greenhouse gases  
571 and aerosols. *Journal of Geophysical Research: Atmospheres*, 120(19), 9837–  
572 9854. <https://doi.org/10.1002/2015JD023364>
- 573 Pincus, R., Forster, P. M., & Stevens, B. (2016). The Radiative Forcing Model  
574 Intercomparison Project (RFMIP): experimental protocol for CMIP6. *Geosci-  
575 entific Model Development*, 9(9), 3447–3460. [https://doi.org/10.5194/gmd-9-  
576 3447-2016](https://doi.org/10.5194/gmd-9-3447-2016)
- 577 Proistosescu, C., & Huybers, P. J. (2017). Slow climate mode reconciles histori-  
578 cal and model-based estimates of climate sensitivity. *Sciences Advances*, 3,  
579 e1602821. <https://doi.org/10.1126/sciadv.1602821>
- 580 Rohrschneider, T., Stevens, B., & Mauritsen, T. (2019). On simple representations  
581 of the climate response to external radiative forcing. *Climate Dynamics*, 53(5),  
582 3131–3145. <https://doi.org/10.1007/s00382-019-04686-4>
- 583 Rugenstein, M., Bloch-Johnson, J., Gregory, J., Andrews, T., Mauritsen, T., Li, C.,  
584 ... Knutti, R. (2020). Equilibrium Climate Sensitivity Estimated by Equili-  
585 brating Climate Models. *Geophysical Research Letters*, 47(4), e2019GL083898.  
586 <https://doi.org/10.1029/2019GL083898>
- 587 Rugenstein, M., Caldeira, K., & Knutti, R. (2016). Dependence of global radi-  
588 ative feedbacks on evolving patterns of surface heat fluxes. *Geophysical Research  
589 Letters*, 43(18), 9877–9885. <https://doi.org/10.1002/2016GL070907>
- 590 Rugenstein, M., Gregory, J. M., Schaller, N., Sedláček, J., & Knutti, R. (2016). Mul-  
591 tiannual Ocean–Atmosphere Adjustments to Radiative Forcing. *Journal of Cli-  
592 mate*, 29(15), 5643–5659. <https://doi.org/10.1175/JCLI-D-16-0312.1>
- 593 Rypdal, M., & Rypdal, K. (2014). Long-Memory Effects in Linear Response Models  
594 of Earth’s Temperature and Implications for Future Global Warming. *Journal  
595 of Climate*, 27, 5240–5258. <https://doi.org/10.1175/JCLI-D-13-00296.1>
- 596 Sherwood, S. C., Bony, S., Boucher, O., Bretherton, C., Forster, P. M., Gregory,  
597 J. M., & Stevens, B. (2015). Adjustments in the Forcing-Feedback Framework  
598 for Understanding Climate Change. *Bulletin of the American Meteorological  
599 Society*, 96(2), 217–228. <https://doi.org/10.1175/BAMS-D-13-00167.1>
- 600 Smith, C. J., Kramer, R. J., Myhre, G., Alterskjær, K., Collins, W., Sima, A.,  
601 ... Forster, P. M. (2020). Effective radiative forcing and adjustments in  
602 cmip6 models. *Atmospheric Chemistry and Physics*, 20(16), 9591–9618.  
603 <https://doi.org/10.5194/acp-20-9591-2020>
- 604 Soden, B. J., Collins, W. D., & Feldman, D. R. (2018). Reducing  
605 uncertainties in climate models. *Science*, 361(6400), 326–327.  
606 <https://doi.org/10.1126/science.aau1864>
- 607 Tang, T., Shindell, D., Faluvegi, G., Myhre, G., Olivié, D., Voulgarakis, A., ...

- 608 Smith, C. (2019). Comparison of Effective Radiative Forcing Calculations Us-  
609 ing Multiple Methods, Drivers, and Models. *Journal of Geophysical Research:*  
610 *Atmospheres*, *124*(8), 4382-4394. <https://doi.org/10.1029/2018JD030188>
- 611 Trossman, D. S., Palter, J. B., Merlis, T. M., Huang, Y., & Xia, Y. (2016).  
612 Large-scale ocean circulation-cloud interactions reduce the pace of tran-  
613 sient climate change. *Geophysical Research Letters*, *43*(8), 3935–3943.  
614 <https://doi.org/10.1002/2016GL067931>
- 615 Williams, K. D., Ingram, W. J., & Gregory, J. M. (2008). Time Variation of Ef-  
616 fective Climate Sensitivity in GCMs. *Journal of Climate*, *21*(19), 5076-5090.  
617 <https://doi.org/10.1175/2008JCLI2371.1>
- 618 Winton, M., Takahashi, K., & Held, I. M. (2010). Importance of Ocean Heat Uptake  
619 Efficacy to Transient Climate Change. *Journal of Climate*, *23*(9), 2333-2344.  
620 <https://doi.org/10.1175/2009JCLI3139.1>
- 621 Zelinka, M. D., Klein, S. A., Taylor, K. E., Andrews, T., Webb, M. J., Gregory,  
622 J. M., & Forster, P. M. (2013). Contributions of Different Cloud Types to  
623 Feedbacks and Rapid Adjustments in CMIP5. *Journal of Climate*, *26*(14),  
624 5007–5027. <https://doi.org/10.1175/JCLI-D-12-00555.1>
- 625 Zelinka, M. D., Myers, T. A., McCoy, D. T., Po-Chedley, S., Caldwell, P. M.,  
626 Ceppi, P., . . . Taylor, K. E. (2020). Causes of Higher Climate Sensitivity  
627 in CMIP6 Models. *Geophysical Research Letters*, *47*(1), e2019GL085782.  
628 <https://doi.org/10.1029/2019GL085782>
- 629 Zhou, C., Zelinka, M. D., Dessler, A. E., & Klein, S. A. (2015). The relationship  
630 between interannual and long-term cloud feedbacks. *Geophysical Research Let-*  
631 *ters*, *42*(23), 10,463-10,469. <https://doi.org/10.1002/2015GL066698>
- 632 Zhou, C., Zelinka, M. D., & Klein, S. A. (2016). Impact of decadal cloud vari-  
633 ations on the Earth’s energy budget. *Nature Geoscience*, *9*(12), 871–874.  
634 <https://doi.org/10.1038/ngeo2828>